



REGULAR ARTICLE

Study and Performance Improvement of Ultrathin CIGS Solar Cells

B. Kaghouche^{1,2*} , A. Saouli^{1,3}, I. Nouicer⁴, S. Abadli², Z. Deridj², S. Boulmelh², L. Dib², L. Saci²

¹ Abdelhafid Boussouf University centre of Mila, BP N°26 RP Mila 43000, Algeria

² LEMEAMED Laboratory, Electronics Department, University of Constantine 1 – Mentouri Brothers, 25000 Constantine, Algeria

³ Microsystems and Instrumentation Laboratories (LMI), Faculty of Technology Sciences, Mentouri Brothers University of Constantine, 25000 Constantine, Algeria

⁴ Centre de Développement des Energies Renouvelables, (CDER), B.P. 62, Route de l'Observatoire, 16340, Bouzaréah, Algiers, Algeria

(Received 05 August 2025; revised manuscript received 11 December 2025; published online 19 December 2025)

The second generation solar cells based on CIGS absorber layer have significant potential in the photovoltaic field and as we know the current and major challenge of this technology is reducing the CIGS layer thickness in order to minimize the manufacturing cost especially by reducing the consumption of Gallium and Indium which are considered expensive materials. With this in mind, we conducted a simulation study using the ATLAS-SILVACO module in order to optimize the technological parameters and improve the performance of this device. Indeed, based on an ultrathin CIGS cell already produced we were able to fix the technological parameters of the studied cell. The efficiency and the form factor are almost in perfect agreement with the reference solar cell ($\eta = 8.62\%$ and $FF = 58\%$). The defect density in the absorber structure was studied. We attributed the increase in defect density (of the order of 10^{15} cm^{-3}) to the increase in grain boundaries density. We discussed the effect of the abundant presence of the Copper Cu in ultrathin CIGS solar cell. Then, the introduction of a 25 nm thick Al_2O_3 passivation layer with negative fixed charges at the CIGS/ Al_2O_3 interface allowed an improvement in the device performance where we recorded an efficiency $\eta = 11.22\%$ and $FF = 64\%$. Finally, we conducted an optimization based on the introduction of a P^+ -CIGS BSF layer. The evolution of the electrical characteristics of the ultrathin solar cell was discussed as a function of the acceptor density and the BSF layer thickness. This AZO/ i -ZnO/CdS/ P -CIGS/ P^+ -CIGS/Mo configuration allowed to estimate an increase in efficiency up to $\eta = 15.47\%$ ($FF = 73.46\%$).

Keywords: Ultrathin CIGS, ATLAS-SILVACO, Defect density, Passivation, Pitch, BSF.

DOI: [10.21272/jnep.17\(6\).06005](https://doi.org/10.21272/jnep.17(6).06005)

PACS numbers: 73.50.Pz, 85.30.De

1. INTRODUCTION

The photovoltaic industry is currently experiencing the development of second-generation solar cells based on chalcopyrite structure, which has made it possible to use thinner absorber materials of the order of 2 μm such as CZTSe and CIGS [1-3] instead of 200 μm for Si-based cells. These materials have made it possible to have efficiency greater than 20% [4-5] while reducing the thickness of the solar cell, which minimizes the cost and preserves materials. Current research is particularly focused on optimizing the cell stack and in particular reducing the thickness of the absorber. Indeed, for an AZO/ZnO/CdS/CIGS/Mo stack, current research has shown that an efficiency of 8% can be achieved with a thickness of 360 nm [6]. G. Rajan et al [7] obtained for the same stack an efficiency of 8.6% with a CIGS thickness equal to 350 nm. Moreover, many studies have shown that the thickness of 500 nm cannot be overcome because beyond that the cell performance will drastically degrade the performance [6-8], namely the presence of

shunting effects which are due to the presence of certain quantities of Copper Cu, the decrease in absorption linked to the reduction in the thickness of the absorber, the increase in defects which increases the recombination of electron-hole pairs especially on the rear surface. The rear passivation using different insulators (Al_2O_3 , SiO_2 , HfO_2 , ... etc.) [8-10] has made it possible to reduce rear surface recombination as well as defects. Indeed, Lontchi Jiole et al [11] for a thickness of 500 nm of the absorber, achieved an efficiency of 12.68% by introducing a 25 nm layer of Al_2O_3 , this by the presence of a negative charge density Q_f at the CIGS/ Al_2O_3 interface equal to cm^{-2} . Bourkott et al [9] showed that the efficiency can be improved up to 13.53% if the charge density at the CIGS/ Al_2O_3 interface is cm^{-2} . With this in mind, we will conduct a study based on simulation by the ATLAS tool of TCAD-SILVACO in order to remedy the shunting problems as well as the constraints related to recombination on the rear surface, which will lead to the improvement of the ultrathin CIGS solar cell performance. Initially, the proposed model was validated

* Correspondence e-mail: b.kaghouche@centre-univ-mila.dz



against a similar ultrathin structure already realized by G.Rajan et al [7]. Then, the parameters affecting the performance of the ultrathin cell will be discussed and in particular the structural defects and the shunting effects caused by the presence of Cu in the CIGS absorber. Finally, the technological optimizations made to this structure will be highlighted.

2. DEVICE STRUCTURE AND NUMERICAL MODELING

The study was based on the 2D simulation of the ultrathin CIGS solar cell using ATLAS-SILVACO software. It is important to note that the accuracy of device simulations by TCAD-SILVACO software depends significantly on the input data and in particular, the models chosen to describe the physical and electrical behavior of these devices. Indeed, to account for the physical and optoelectronic phenomena that occur in our solar cell structure, we used the basic equations: the Poisson equation, the continuity equation and the transport equation as well as the three recombination mechanisms (Shockley-Read-Hall (SRH) Recombination, Auger Recombination and Optical Generation/Radiative Recombination). These mechanisms play a crucial role when modeling a second generation solar cell [12] but the SRH mechanism remains predominant compared to the others in the CIGS solar cell.

The equation for calculating Shockley-Read-Hall (SRH) Recombination R_{SRH} is given as follows [12]:

$$R_{SRH} = \frac{pn - n_{ie}^2}{T_{P0} \left[n + n_{ie} e^{\left(\frac{E_{TP}}{k.T_L}\right)} \right] + T_{N0} \left[p + n_{ie} e^{\left(\frac{E_{TP}}{k.T_L}\right)} \right]} \quad (1)$$

Where, E_{TP} is the difference between the trap energy level and the intrinsic Fermi level, T_{P0} and T_{N0} are the electron and hole lifetimes, n_{ie} is the effective intrinsic concentration, p and n are carrier concentration, k is the Boltzmann's constant and T_L is the lattice temperature in degrees Kelvin.

The cell studied is composed of the AZO/ZnO/CdS/CIGS/Mo stack illustrated in Figure 1.

To validate our ATLAS SILVACO simulation results we adopted the structure proposed by G. Rajan et al [7] where a layer of *P*-doped Cu(In, Ga)Se₂ (CIGS) with a thickness of 350 nm was deposited on the Molybdenum.



Fig. 1 – The Ultrathin CIGS solar cell structure

In order to form the *PN* junction we deposited on the absorber material a buffer layer of CdS (50 nm). Then, we

deposited a layer of intrinsic ZnO (200 nm). Finally, the window layer is carried out by depositing aluminum-doped ZnO (AZO) with a thickness of 300 nm onto the *i*-ZnO. The physical and technological parameters of the different materials used in this structure are summarized in Table 1.

The efficiency of this cell is highly dependent on the CIGS absorber material and especially when this cell is considered ultrathin. Indeed, several studies have detailed the different processes for producing Cu(In, Ga)Se₂ [1,10]. The presence of the four materials Cu, In, Ga and Se in the CIGS structure plays a determining role. This is controlled by the ratios $x = [Ga]/([In] + [Ga])$ and $y = [Cu]/([In] + [Ga])$, the ratio x allows the adjustment of the bandgap E_g between 1.04 eV and 1.67 eV [14]. The ratio $[Cu]/([In] + [Ga])$ allows to control the enrichment and depletion of Copper Cu in the structure [15]. It should be noted that the bandgap of CIGS material used in this structure is 1.12 eV [7].

Table 1 – Material properties [2, 5]

Parameters	AZO	<i>i</i> -ZnO	CdS	CIGS
Thickness (nm)	300	200	50	350
Bandgap (eV)	3.44	3.37	2.4	varied
Dielectric permittivity	9	9	10	13.6
Electron affinity	4.55	4.55	4.45	3.89
N_c (cm ⁻³)	2.2E18	2.2E18	2.2E18	2.2E18
N_v (cm ⁻³)	1.8E19	1.8E19	1.8E19	1.8E19
Electron mobility μ_n (cm ² /Vs)	100	100	100	100
Hole mobility μ_p (cm ² /Vs)	25	25	25	25
Donor density (cm ⁻³)	1E18	–	6E17	–
Acceptor density (cm ⁻³)	–	–	–	1E17
Defect density (cm ⁻²)	1E17	1E17	1E17	1E15

The bandgap E_g (eV) can be calculated from the following relation [14]:

$$E_g = 1.04 + 0.63x + 0.21x(1 - x) \quad (2)$$

3. RESULTS AND DISCUSSION

Comparing the obtained results for an ultrathin CIGS solar cell with an absorber thickness equal to 350 nm to those found in the literature [7], it can be said that electrical characteristics obtained by ATLAS-SILVACO are appropriate and quite consistent (see Table 2). Note that the simulations carried out in this study are compliant with STC conditions.

Table 2 – Extracted parameters of Ultrathin CIGS solar cell

Parameters	Experimental [6]	Simulation
V_{oc} (V)	0.5	0.56
I_{cc} (mA/cm ²)	28.1	29.12
FF (%)	61	58
η (%)	8.6	8.62

The degradation of ultrathin CIGS solar cell performance (absorber thickness equal to 350 nm, $\eta = 8.62\%$) compared to a thin CIGS cell (absorber thickness = 2 μm , $\eta = 21\%$,) [16] can be clearly seen as the thickness is reduced. This is directly due to the grain boundary interfaces which are considered positively charged structural defects. These positively charged defects will significantly increase the recombination rate in the absorber layer especially in the rear surface (see Figure 2). Several studies have linked the degradation of ultrathin CIGS solar cells performance to the increase in the rear surface recombination [6, 10, 17]. But in reality and as shown in the Figure 2, we cannot neglect the impact of the defect density in the quasi neutral zone of CIGS because the increase in the defect density in the absorber leads to an increase in the recombination rate and consequently the degradation of the ultrathin CIGS solar cell performance. As shown in Table 3, the increase in defect density leads to the decrease in the device efficiency. The increase in defect density can be related to the decrease in grain size. Indeed, G. Rajan et al. [7] revealed that in a 3-step process for manufacturing ultrathin CIGS films, the reduced deposition time implies a decrease in the CIGS grain size. This decrease will lead

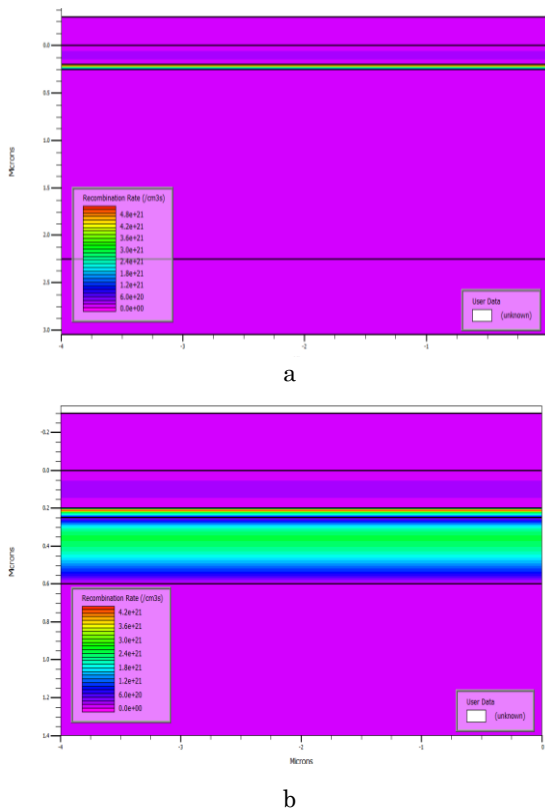


Fig.2 – Recombination evolution in the solar cell: (a) thickness of CIGS absorber 2 μm , (b) thickness of CIGS absorber 0.35 μm

Table 3 – Extracted parameters of defect density effect on 350 nm absorber CIGS

Defect density (cm ⁻²)	V_{oc} (V)	J_{sc} (mA·cm ⁻²)	η (%)	FF(%)
10 ¹⁰	0.57	29.33	9.18	60.76
10 ¹²	0.57	29.33	9.18	60.76
10 ¹⁴	0.57	29.31	9.12	60.49
10 ¹⁵	0.56	29.12	8.62	58
10 ¹⁶	0.53	27.63	6.21	46.80

to an increase in the density of grain boundaries and consequently the increase in the density of defects in the structure. It should be noted that the defect density of 10¹⁵ cm⁻³ allowed for good agreement between the experimental and theoretical data.

Figure 3 illustrates the evolution of the efficiency (and Fill Factor) as a function of the acceptor density N_A . It can be seen that the efficiency of the ultrathin cell increases from 7.90 % to 9.20 % (the Fill Factor increases from 52.95 % to 66 %) when the acceptor density varies from 10¹⁵ cm⁻³ to 10¹⁷ cm⁻³. This improvement can be attributed to the copper weakening because the increase in *P*-type doping in these films is accompanied by the creation of more Cu vacancies V_{Cu} [18]. Therefore, the presence of more copper in the Ultrathin CIGS cells produces shunting effects in the structure.

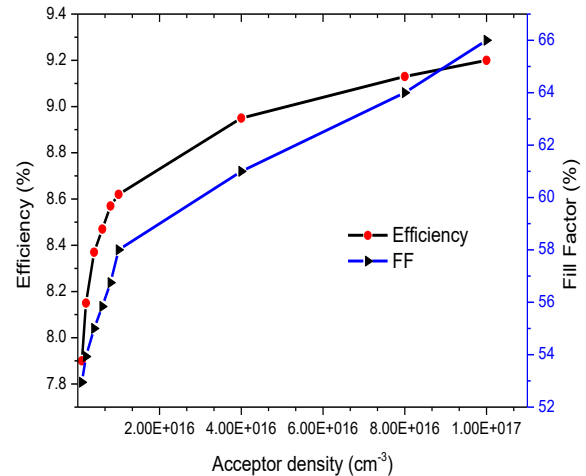


Fig. 3 – Efficiency and Fill Factor versus Absorber carrier concentration

In order to reduce the recombination that occur at the rear surface of the structure, we proceeded to deposit on the molybdenum an alumina passivation layer (Al_2O_3) with 200 nm contact openings (itches) [6, 8, 9] (see Figure 4(a)). A study carried out by S. Bose et al. [8] demonstrated that the introduction of a 25 nm thick alumina passivation layer with pitches of about 200 nm in an ultrathin CIGS solar cell with an absorber thickness of 500 nm allowed having an increase in efficiency from 8.1 % to 9.5 %, i.e., an improvement of 14.73 %. The Figure 4(b) clearly shows the decrease in the recombination rate at the rear surface compared to the basic structure (see Figure 2(b)). The introduction of the alumina layer led to a passivation of donor defects by reducing Se vacancy defect. The reduction of donor defects will thus increase the electric field which leads to reducing the

effective interface recombination velocity. Several studies have recorded the presence of negative fixed charge at the CIGS/Al₂O₃ interface with a density of the order of 10¹² cm⁻² [9, 11].

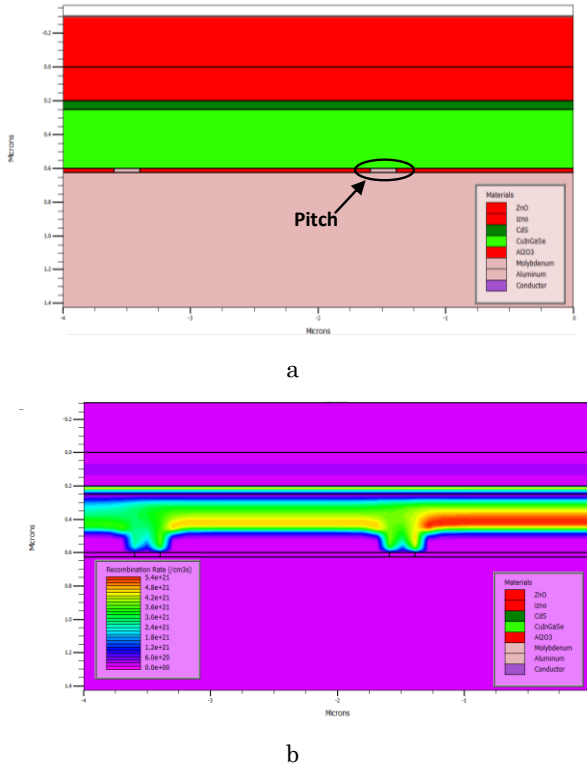


Fig.4–Rear surface passivation:(a) simulated structure, (b) Recombination rate after passivation

These negative charges have contributed to the improvement of the characteristics, with the highest efficiency of 11.22 % being the one that has more fixed charges at the CIGS/Al₂O₃ interface (see Figure 5). However, although we recorded an increase in efficiency with increasing negative fixed charges at the CIGS/Al₂O₃ interface, the efficiency value remains stable beyond $Q_f = 7 \times 10^{12}$ cm⁻².

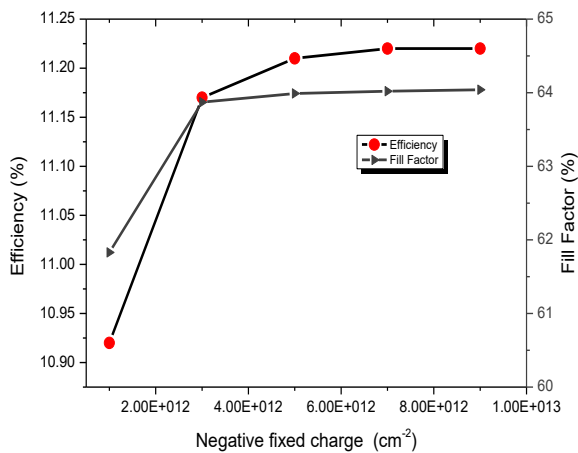


Fig. 5 – Effect of negative fixed charge on electrical parameters of solar cell

Figure 6 describes the evolution of the electric field at the rear contact as a function of the fixed charges that appear at the absorber/insulator interface. We can see that the existence of the negative fixed charges at the CIGS/Al₂O₃ interface, when they vary from 10¹² cm⁻³ to 9.10¹² cm⁻³, has allowed increasing the electric field from 34 kV/cm to 71 kV/cm.

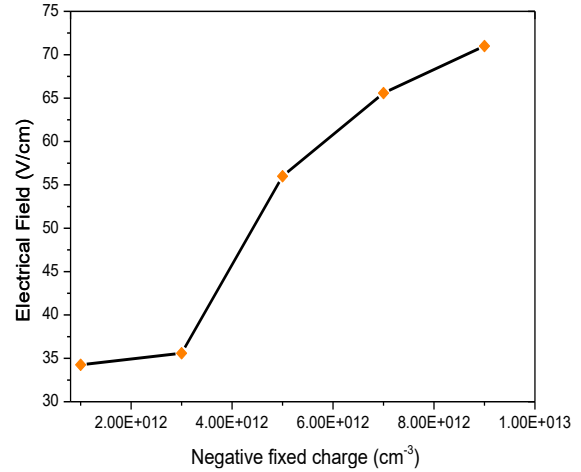


Fig. 6 – Effective electric field at the absorber close to the rear contact

In order to improve the performance of ultrathin CIGS solar cells, we were initially fixed acceptor density $N_A = 10^{17}$ cm⁻³. Then we were interested in optimizing the absorber bandgap, we remind that the CIGS Bandgap used in the G. Rajan et al. [7] structure is of the order of 1.12 eV. In theory, increasing the bandgap makes it possible to increase the efficiency of CIGS solar cells by increasing the V_{oc} . Indeed, we found that when the gap varies between 1.12 and 1.4 eV (see Figure 7), the efficiency increased by 11.22 % to 15.06 %. But in practice, when the gap exceeds 1.27, the battery experiences a degradation of its performance due to the increase in structural defects [19]. So the presence of more Gallium at the expense of Indium will lead to a growth of defect density. Indeed, for an ultrathin CIGS cell and in order to reduce the defect density in the structure, it is suggested to opt for a bandgap value of approximately 1.23 eV [6,10], This choice allowed to have an improvement of the efficiency $\eta = 14.08$ % (FF = 70.98 %) which corresponds to an improvement of $\Delta\eta = 38.77$ % while retaining the value of the defects density already optimized during the validation of the technological parameters of the cell studied.

In order to further improve the ultrathin solar cell performance, we used a highly doped layer as the Back Surface Field (BSF) layer. Several works have demonstrated that the introduction of a highly acceptor doping layer between the rear contact and the CIGS absorber such as Si, SnS, ZnSe, PbS [20-24] has made it possible to increase the efficiency of the solar cell. Based on the fact that reducing the deposition time leads to an increase in the defect density, we opted for the integration of a BSF P⁺-CIGS layer, i.e, the same CIGS absorber material, while maintaining the same initial thickness of 350 nm. Therefore, the deposition time will be preserved and the density of defects will not be affected.

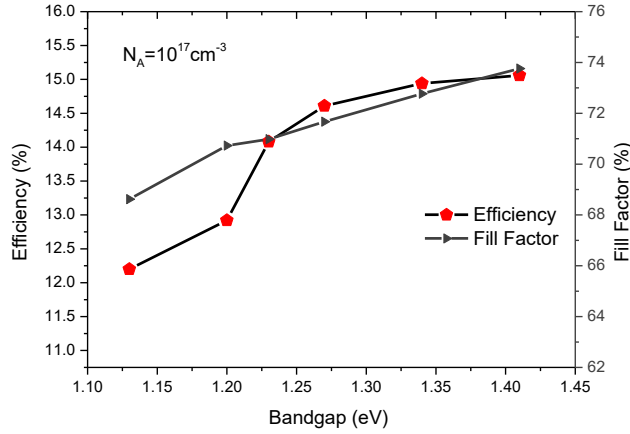


Fig. 7 – Evolution of solar cell Efficiency and Fill Factor at various bandgap values

Table 5 illustrates the evolution of the ultrathin solar cell performance as a function of the doping density of the BSF layer (the BSF layer thickness equals to 50 nm). The obtained results show that when the solar cell electrical characteristics: J_{sc} , V_{oc} , η and FF increase with the increase of the BSF layer acceptor density. The highest efficiency is $\eta = 15.04\%$ which corresponds to the doping density $N_{\text{ABSF}} = 10^{20} \text{ cm}^{-3}$. We can see that the yield begins to decrease from the concentration $N_{\text{ABSF}} = 10^{21} \text{ cm}^{-3}$. This improvement is due to the addition of an electric field on the back surface. Indeed, the introduction of the P^+ -CIGS layer on the back surface between the passivation layer and the absorber (P -CIGS) created a repulsive electric field resulting from a (P/P^+) junction. This electric field allowed, on the one hand, to reduce the rear surface recombination, on the other hand, to propel the electrons which are considered as minority carriers towards the front contact. This can be explained by the increase in the short-circuit current density J_{sc} which increased from 28.37 mA/cm^2 to 29.35 mA/cm^2 .

Table 5 – Estimated electrical characteristics after introducing a 50 nm thick BSF layer for different acceptor concentrations

Acceptor density of P^+ -CIGS layer $N_{\text{ABSF}} (\text{cm}^{-3})$	V_{oc} (V)	J_{sc} ($\text{mA}\cdot\text{cm}^{-2}$)	$\eta(\%)$	FF(%)
Without BSF Layer	0.751	28.37	14.08	70.98
10^{18}	0.756	29.12	14.74	71.92
10^{19}	0.758	29.35	14.99	72.39
10^{20}	0.758	29.37	15.04	72.53
10^{21}	0.758	28.95	14.86	72.66

The effect of the BSF layer thickness as a function of the acceptor density was also optimized (see Table 6), we

found that the thickness of $d_{\text{BSF}} = 100 \text{ nm}$ with the doping density $N_{\text{ABSF}} = 10^{19} \text{ cm}^{-3}$ of the BSF layer allowed to have the best efficiency which corresponds to $\eta = 15.47\%$.

Table 6 – The ultrathin CIGS solar cell electrical characteristics as a function of the BSF layer thickness and acceptor density

d_{BSF} (nm)	$N_{\text{ABSF}} = 10^{19} \text{ cm}^{-3}$		$N_{\text{ABSF}} = 10^{20} \text{ cm}^{-3}$	
	$\eta (\%)$	FF(%)	$\eta (\%)$	FF(%)
50	14.99	72.39	15.04	72.53
100	15.47	73.46	15.34	73.65
150	15.26	76.44	14.55	76.79

4. CONCLUSION

In this study we investigated an ultrathin CIGS-based solar cell. The study was carried out using the simulation with ATLAS-SILVACO. Initially, we validated our results including the technological parameters based on the structure realized by G. Rajan et al. [6]. The optimization of the technological parameters allowed to have a yield $\eta = 8.62\%$. As a crucial technological parameter, we found that the defect density is of the order of 10^{15} cm^{-2} , this is related to the increase in the grain boundaries density caused by the formation of small-sized grains. We fixed the CIGS absorber layer according to the presence of copper in the CIGS structure. Then, in order to improve the performance of this stack, we carried out a passivation with a 25 nm layer of Al_2O_3 with contact pitches of 200 nm. The passivation allowed to obtain an improvement in the efficiency of $\Delta\eta = 14.7\%$. This was explained by the decrease in the rear surface recombination. Furthermore, we have confirmed the presence of negative fixed charges of the order of cm^{-2} at the CIGS/ Al_2O_3 interface. Then, we proceeded to improve the ultrathin CIGS solar cell performance by optimizing some physical and technological parameters. We found that the optimal acceptor density of the absorber is of the order of 10^{17} cm^{-3} . As for the CIGS material bandgap, the correlation between the calculated results and the experimental results presented in the literature allowed us to take into consideration $E_g = 1.23 \text{ eV}$. Finally, in order to further reduce the rear surface recombination, we proposed to add a BSF layer (P^+ -CIGS) while keeping the same initial thickness ($d_{\text{BSF}} + d_{\text{CIGS}} = 350 \text{ nm}$). This configuration allowed adding an electric field which led to reduce the recombination which occurs on the rear surface, and consequently the increase in the passage of minorities (electrons) towards the rear contact (increase of the J_{sc}). Finally, an optimization of the BSF layer thickness and acceptor density was carried out. We found that the pair $d_{\text{BSF}} = 100 \text{ nm}$ and $N_{\text{ABSF}} = 10^{19} \text{ cm}^{-3}$ allowed to obtain a maximum efficiency $\eta = 15.47\%$.

REFERENCES

1. S. Rahimi, M. Shooshtari, *Appl. Sci.* **12**, 4119 (2022).
2. A. Khadir, *Opt. Mater.* **108**, 110443 (2020).
3. A.K. Patel, R. Mishra, S.K. Soni, *Sol. Energy* **257**, 125 (2023).
4. P. Jackson, D. Hariskos, E. Lotter, S. Paetel, R. Wuerz, R. Menner, W. Wischmann, M. Powalla, *Prog. Photovolt: Res. Appl.* **19**, 894 (2010).
5. S. Gohri, J. Madan, Rahul Pandey, *J. Electron. Mater.* **52**, 6335 (2023).
6. J. Krc, G. Cernivec, A. Campa, J. Malmstrom, M. Edoff, F. Smole, M. Topic, *Opt. Quant. Electron.* **38** (12-14), 1115 (2007).
7. G. Rajan, K. Aryal, S. Karki, P. Aryal, R.W. Collins, S. Marsillac, *J. Spectroscopy* **2018**, 8527491 (2018).
8. S. Bose, J.M.V. Cunha, J. Borme, W.C. Chen, N.S. Nilsson, J.P. Teixeira, J. Gaspa, J.P. Leitão, M. Edoff, P.A. Fernandes, P.M.P. Salomé, *Thin Solid Films* **671**, 77 (2019).
9. Ziang Cao, Fangfang Mei, Dashan Zhang, Bingyou Liu, Yuwei Wang, Wenhui Hou, *Electronics* **12**, 785 (2023).
10. K. Oliveira, J. Teixeira, W. Chen, J. Lontchi, A. Oliveira, I. Čaha, *IEEE J. Photovoltaic.* **12** No 4, 954 (2024).
11. J. Lontchi, M. Zhukova, M. Kovacic, J. Krc, W. Chen, M. Edoff, S. Bose, P. Salome, J. Goffard, A. Cattoni, L. Gouillart, S. Collin, V. Gusak, D. Flandre, *IEEE J. Photovoltaic.* **10**, 1908 (2020).
12. Silvaco, ATLAS User's Manual Device Simulation Software, St. Clara, CA.
13. J. Goffard, C. Colin, F. Mollica, A. Cattoni, C. Sauvan, Philippe Lalanne, J. Guillemoles, N. Naghavi, S. Collin, *IEEE J. Photovoltaic.* **7** No 5, 1433 (2017).
14. X. Lv, Z. Zheng, M. Zhao, H. Wang, Daming Zhuang, *Materials* **16**, 2806 (2023).
15. J. Ramanujam, U. Singh, *Energy Environ. Sci.* **10**, 1306 (2017).
16. C. Zhao, S. Yu, W. Tang, X. Yuan, H. Zhou, T. Qi, X. Zheng, D. Ning, M. Ma, J. Zhu, J. Zhang, C. Yang, W. Li, *Mater. Rep.: Energy* **3**, 100214 (2023).
17. N. Boukourt, S. Patané, M. Adouane, *Electronics* **12**, 758 (2023).
18. G.F. Novikov, E.V. Rabenok, P.S. Orishina, M.V. Gapanovich, I.N. Odin, *Electron. Prop. Semiconductor.* **53**, 323 (2019).
19. D. Abou-Ras, R. Caballero, C.A. Kaufmann, M. Nichterwitz, K. Sakurai, S. Schorr, T. Unold, H.W. Schock, *phys. status solidi (RRL) – Rapid Res. Lett.* **2** No 3, 135 (2008).
20. Z. Benbouzid, W. Benstaali, W.L. Rahal, N. Hassini, M.R. Benzidane, A. Boukourt, *J. Electron. Mater.* **52**, 4575 (2023).
21. S. Souri, M. Marandi, *Opt. Quantum Electron.* **55**, 397 (2023).
22. S.A.M. Ziabari, A.A. Ziabari, S.J. Mousavi, *J. Comput. Electron.* **21**, 675 (2022).
23. R. Zouache, I. Bouchama, O. Saidani, L. Djedoui, E. Zaidi, *J. Comput. Electron.* **21**, 1386 (2022).

Дослідження та покращення продуктивності ультратонких сонячних елементів CIGS

B. Kaghouche^{1,2}, A. Saouli^{1,3}, I. Nouicer⁴, S. Abadli², Z. Deridj², S. Boulmelh², L. Dib², L. Saci²

¹ Abdelhafid Boussouf University centre of Mila, BP N°26 RP Mila 43000, Algeria

² LEMEAMED Laboratory, Electronics Department, University of Constantine 1 – Mentouri Brothers, 25000 Constantine, Algeria

³ Microsystems and Instrumentation Laboratories (LMI), Faculty of Technology Sciences, Mentouri Brothers University of Constantine, 25000 Constantine, Algeria

⁴ Centre de Développement des Energies Renouvelables, (CDER), B.P. 62, Route de l'Observatoire, 16340, Bouzaréah, Algiers, Algeria

Сонячні елементи другого покоління на основі поглинального шару CIGS мають значний потенціал у фотоелектричній галузі, і, як ми знаємо, головним викликом цієї технології є зменшення товщини шару CIGS з метою мінімізації виробничих витрат, особливо шляхом зменшення споживання галію та індію, які вважаються дорогими матеріалами. З огляду на це, ми провели моделювання з використанням модуля ATLAS-SILVACO, щоб оптимізувати технологічні параметри та покращити продуктивність цього пристрою. Дійсно, на основі вже виготовленого надтонкого елемента CIGS нам вдалося зафіксувати технологічні параметри досліджуваного елемента. Ефективність та форм-фактор майже ідеально узгоджуються з еталонним сонячним елементом ($\eta = 8,62\%$ та $FF = 58\%$). Була досліджена щільність дефектів у структурі поглинача. Збільшення щільності дефектів (порядку 10^{15} cm^{-3}) ми пов'язали зі збільшенням щільності меж зерен. Ми обговорили вплив великої кількості міді (Cu) в надтонкому сонячному елементі CIGS. Потім, введення шару пасивації Al_2O_3 товщиною 25 нм з негативними фіксованими зарядами на межі розділу CIGS/ Al_2O_3 дозволило покращити продуктивність пристрою, де ми зафіксували ефективність $\eta = 11,22\%$ та $FF = 64\%$. Нарешті, ми провели оптимізацію на основі введення шару P^+ -CIGS BSF. Еволюцію електричних характеристик ультратонкого сонячного елемента обговорювали як функцію щільності акцептора та товщини шару BSF. Ця конфігурація AZO/ $\text{ZnO}/\text{CdS}/P^+$ -CIGS/ P^+ -CIGS/Мо дозволила оцінити збільшення ефективності до $\eta = 15,47\%$ ($FF = 73,46\%$).

Ключові слова: Ультратонкі CIGS, ATLAS-SILVACO, Щільність дефектів, Пасивація, BSF.